The Impact of Tropical Storm Paul (1999) on the Motion and Rainfall Associated with Tropical Storm Rachel (1999) near Taiwan

CHUN-CHIEH WU

Department of Atmospheric Sciences, National Taiwan University, Taipei, Taiwan

KEVIN K. W. CHEUNG

Climate Risk Concentration of Research Excellence, and Department of Environment and Geography, Macquarie University, Sydney, Australia

JAN-HUEY CHEN AND CHENG-CHUAN CHANG

Department of Atmospheric Sciences, National Taiwan University, Taipei, Taiwan

(Manuscript received 30 March 2009, in final form 3 August 2009)

ABSTRACT

A heavy rainfall event associated with the passage of Tropical Storm Rachel (1999) over southern Taiwan was studied in which a conceptual model was proposed. In the model, Tropical Storm Paul (1999) plays an important role in impeding the movement of Rachel, thus becoming one of the key factors in enhancing the rainfall amount in southern Taiwan. To further quantify the above concept, a mesoscale numerical model is used to evaluate the influence of Paul on the simulated rainfall associated with Rachel near Taiwan. Sensitivity experiments are performed by removing the circulation of Paul, and/or the large-scale monsoon trough system, where Paul is imbedded. The potential vorticity diagnosis shows that the movement of Rachel is indeed affected by the presence of Paul. Nevertheless, a more detailed analysis shows that it is the presence of the entire monsoon trough that impedes the movement of Rachel and steers the storm toward southwestern Taiwan especially before its landfall. In all, these results generally support the conceptual model with regard to the heavy rainfall mechanism proposed in a previous study. Moreover, this study further points out that it is the circulation associated with both Paul and the entire monsoon trough that affects the movement of Rachel. In addition, the analyses based on the no-terrain simulation depict the relationships among the moisture-rich air from the South China Sea associated with Rachel, relatively dry air from South China, and the mechanism of forming a warm and dry region to the eastern side of the Taiwan terrain, which greatly influences the heavy rainfall distribution in the event.

1. Introduction

The tropical cyclone (TC) is one of the most threatening natural phenomena leading to serious human and economic losses because of its destructive winds and heavy rainfall. Taiwan is usually impacted by an average of about three to four TCs every year. Some of these TCs form in the monsoon trough east of the Philippines, while the others form in the South China Sea (SCS). Even if the TC does not make landfall directly, heavy rainfall can occur in Taiwan because of the interactions between the outer flow associated with the TC, the monsoonal southwesterly, and the complicated topography of Taiwan (Cheung et al. 2008; Chien et al. 2008; Lee et al. 2008; Wu et al. 2009). Moreover, the existence of the Central Mountain Range (CMR) of Taiwan can deflect the direction of an approaching TC, and modify the structure and rainfall distribution (Wu and Kuo 1999; Wu 2001; Wu et al. 2002). Therefore, a weak or small storm may still induce heavy rainfall over Taiwan when the relative locations of the TC and other synoptic systems are favorable. A case in point for rainfall associated with Tropical Storm (TS) Rachel is therefore studied in this paper.

Through analyses of rainfall events in the United States, Europe, and Asia [including TS Rachel (1999)

Corresponding author address: Chun-Chieh Wu, Department of Atmospheric Sciences, National Taiwan University, 1, Sec. 4, Roosevelt Rd., Taipei 106, Taiwan.
E-mail: cwu@typhoon.as.ntu.edu.tw

DOI: 10.1175/2009MWR3021.1

investigated in this study], Lin et al. (2001) have identified four common factors contributing to the occurrence of heavy orographic rainfalls: 1) a conditionally or potentially unstable airstream impinging on the mountains, 2) a very moist low-level jet, 3) a steep mountain, and 4) a quasi-stationary synoptic system to decelerate the convective system over the threatened area. The first three factors are present in the heavy rainfall event in southwestern Taiwan caused by Rachel, and it will be shown that another TS in the area and the monsoon trough play the role of the fourth factor in affecting the motion of Rachel.

The rainfall event associated with Rachel was also simulated in Chiao and Lin (2003) utilizing the U.S. Navy's Coupled Ocean–Atmosphere Mesoscale Prediction System (COAMPS). It was found that the rainfall evolution agreed well with the orographically induced moisture flux convergence. In addition, by comparing the control simulation without terrain in the model it was concluded that the topographic effect played an important role in the entire rainfall event. In particular, their simulation results indicated that the rainfall patterns started at the slope of CMR and subsequently propagated to the coast, which implied that the Taiwan topography also strongly affected the distribution of localized convective cells.

Despite the work in Lin et al. (2001), the role of TS Paul's presence (in 1999) to the northeast of Rachel in impeding the motion of Rachel remains to be investigated. In this study, detailed analysis based on the potential vorticity inversion technique (Wu et al. 2003, 2004) is performed to verify the Paul's contribution to the movement of Rachel. Furthermore, some numerical experiments are specifically designed to examine the rainfall evolution associated with Rachel in two particular aspects. One is the role of Paul and the monsoon trough in which Paul is embedded in the rainfall event, and the other is the asymmetry in the rainfall distribution in southwestern and northeastern Taiwan, which is not trivial given the track of Rachel.

This paper is organized as follows. Section 2 provides a brief introduction to the synopsis of TSs Rachel and Paul. The numerical model used, the initialization methods, and various experiments performed are detailed in section 3. Section 4 presents analysis results by using potential vorticity diagnostics tools for both observational data and simulations that involve the movement of TS Rachel before landfall. In section 5, the rainfall mechanisms of Rachel when it passed through Taiwan are further explored based on various sensitivity experiments that are complementary to those in Chiao and Lin (2003). Last, summary and overall discussions of the study results are given in section 6.

2. Synopsis of Tropical Storms Rachel and Paul

Two TSs formed successively during August 1999 in the western North Pacific (WNP) and SCS, but did not intensify beyond severe levels throughout their lifetime. Tropical Storm Paul developed in a large monsoon gyre environment in the WNP on 3 August, moved northwestward, and attained a maximum intensity of 50 kt when it was located to the east of Okinawa before dissipating in the Yellow Sea (see the best track of Paul in Fig. 9). Tropical Storm Rachel developed as a midget TS in the SCS about 3 days later and moved initially northeastward following the monsoonal southwesterlies (Fig. 1a). Rachel intensified to 35 kt before making landfall in Taiwan, and weakened significantly afterward because of the land effect. When Rachel entered the open water again, it reintensified to 35 kt before recurving northwestward and then dissipated over the cold ocean surface at a high latitude (McPherson and Stapler 1999).

The synoptic environment for the development of the two TSs was a large monsoon gyre in the WNP (Figs. 1a,b). Paul developed in the eastern periphery of the monsoon gyre and later merged with the gyre at about 0000 UTC 6 August (i.e., the start of the numerical simulation in this study). During this merging process, convection in Paul was inactive probably due to the low sea surface temperature at high latitudes. Much convection was located at the monsoon gyre where the moist southwesterlies encountered the easterlies from the subtropical high. In contrast, Rachel was a considerably compact storm. The mesoscale convective system with a diameter of 400–500 km embedded in Rachel accounted for most of its convection.

Although both TSs were relatively weak and did not cause much damage to the regions they passed through, Rachel did bring heavy rainfall to Taiwan, which began as early as 0600 UTC 6 August when the center of the storm was located around 300 km southwest of Taiwan. During the 12-h period after 1200 UTC 6 August, over 100 mm of rain was accumulated in southern Taiwan (Fig. 2a). It is believed that the rainfall in this period was not directly associated with the convection embedded in Rachel but was due to the convection induced by the orographic lifting of the southwesterly conditionally unstable flow that was further strengthened by the approaching storm (Lin et al. 2001). When the mesoscale convective system embedded in Rachel approached the CMR of Taiwan, heavy rainfall started to move inland and the maximum accumulated rainfall in the southern CMR area during 0000–1200 UTC 7 August was as high as 150 mm (Fig. 2b). In addition to the strong convection within the mesoscale convective system and orographic

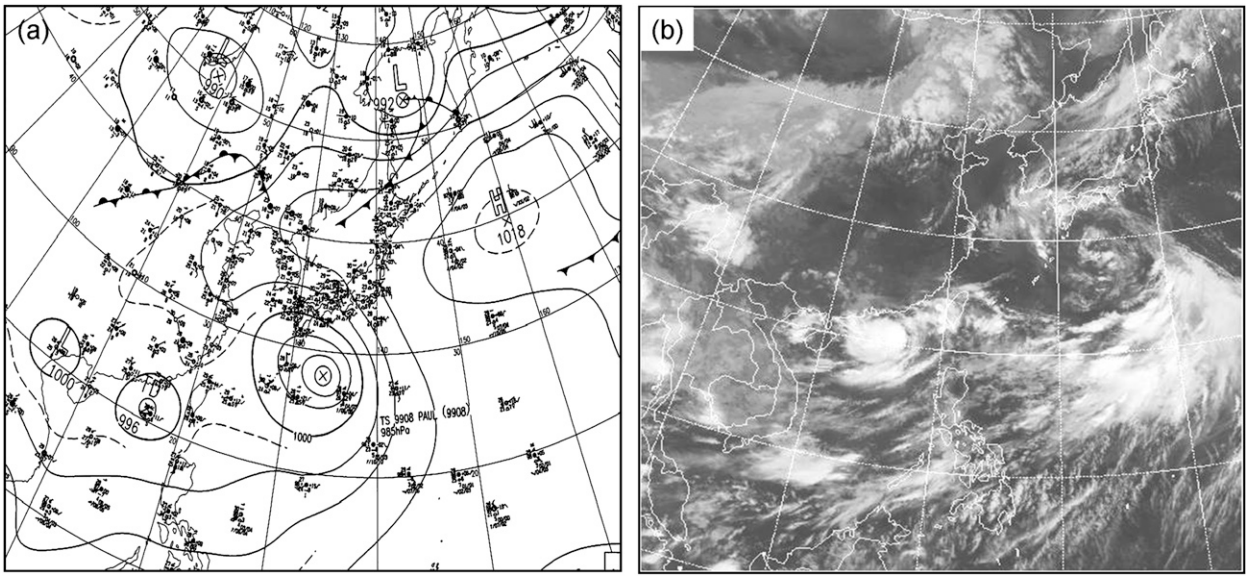

FIG. 1. (a) Japan Meteorological Agency surface weather map, and (b) *GMS-5* infrared satellite imagery at 0000 UTC 6 Aug 1999.

lifting of moist air by the CMR, a crucial factor contributing to the large accumulated rainfall in this period is the deceleration in the movement of Rachel after 0600 UTC 6 August, consistent with the concept that rainfall amount is highly dependent on the speed of the convective system (Doswell et al. 1996). After Rachel made landfall in southwestern Taiwan at about 0600 UTC 7 August, it crossed over the CMR rapidly in the subsequent 6 h and moved to the open ocean northeast of Taiwan. Thus, the accumulated rainfall in northeastern Taiwan was low during the period of 1200 UTC 7 August–0000 UTC 8 August (Fig. 2c). Detailed reasons for this "dryness" in the wake of the TS are explored in section 5.

As Fig. 1 shows, the two TSs were about 20° latitude–longitude apart at 0000 UTC 6 August, and given the large circulation associated with Paul, binary interaction is plausible to explain the subsequent slow movement of Rachel before landfall. However, it is believed that since this can be a typical case study that provides guidance to forecasters in determining the degree of binary interaction between two vortices as compared with other synoptic systems, quantitative diagnosis is necessary.

3. Numerical simulations

a. Initialization methodologies

The fifth-generation Pennsylvania State University–National Center for Atmospheric Research (PSU–NCAR) Mesoscale Model (MM5) is utilized in all numerical simulations in this study. Three domains with horizontal resolution of 54, 18, and 6 km, respectively, are nested as shown in Fig. 3. Physical parameterizations in all three domains are identical, which consist of the mixed-phase microphysics (Reisner et al. 1998), Grell cumulus scheme (Grell 1993), radiation calculation from Dudhia (1993), and the Blackadar boundary layer scheme (Blackadar 1979). Formal integration period is the 48 h during 0000 UTC 6–8 August.

Global analyses from the European Centre for Medium-Range Weather Forecasts (ECMWF) with 1.125° latitude–longitude are input as initial conditions for the MM5 model. To enhance representation of TC vortex circulation in the ECMWF analyses and at the same time maintain dynamical balance with the large-scale fields, the following procedure is applied to initialize TS Rachel. First, a simple Rankine vortex is added to the ECMWF analysis at 1200 UTC 5 August (i.e., 12 h before the formal simulation time) according to the Joint Typhoon Warning Center (JTWC) best-track position and a 12-h simulation is carried out. Then the simulated vortex, which already attains dynamical balance with the embedded synoptic circulation, is separated from the environmental field by the so-called vortex specification algorithm originally developed for the Geophysical Fluid Dynamics Laboratory regional model (Kurihara et al. 1993, 1995). Afterward, the analyzed vortex of Rachel is included into the ECMWF analysis at 0000 UTC 6 August to obtain the initial condition for formal simulation. This procedure is referred to as Spun-up Vortex + Kurihara Filtering (SV + KF) in Table 1. The same procedure is applied to spin up TS Paul except that the final step of

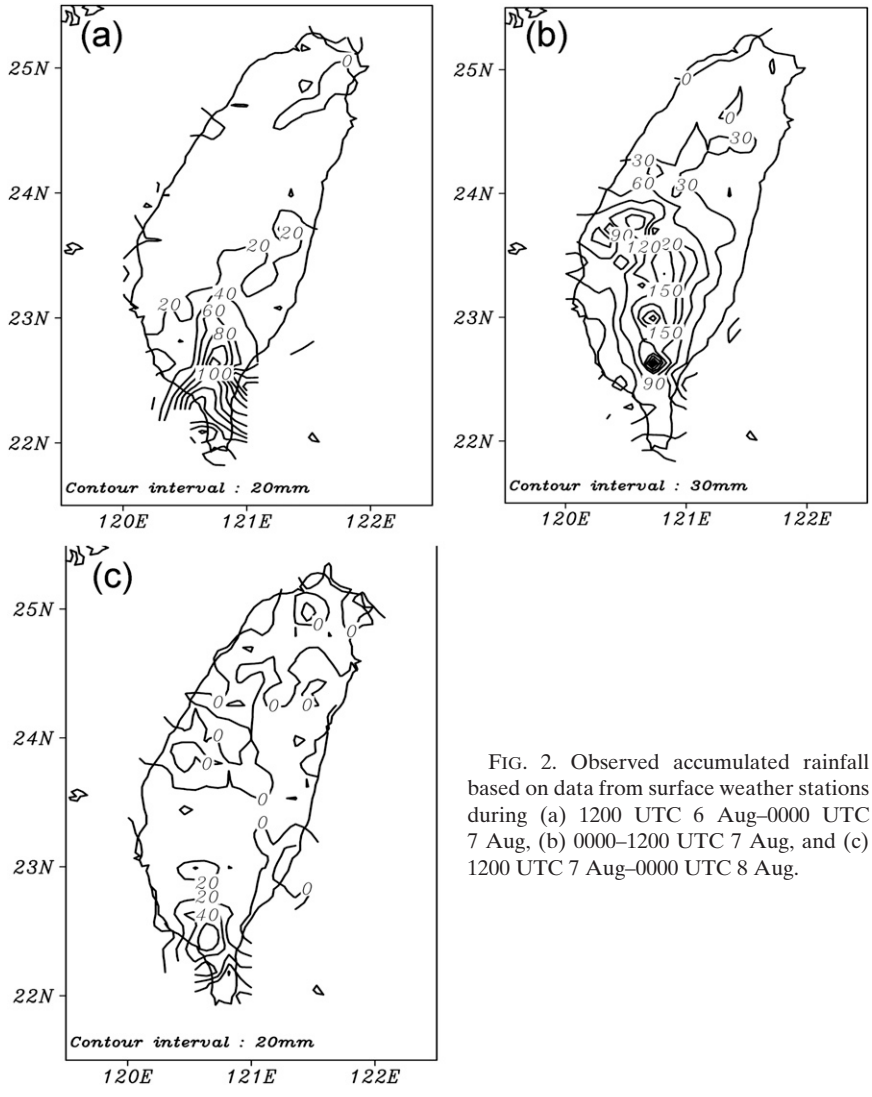

FIG. 2. Observed accumulated rainfall based on data from surface weather stations during (a) 1200 UTC 6 Aug–0000 UTC 7 Aug, (b) 0000–1200 UTC 7 Aug, and (c) 1200 UTC 7 Aug–0000 UTC 8 Aug.

Kurihara filtering for the ECMWF analysis is skipped because the deep trough area of the monsoon gyre remains in the environmental flow after the filtering but with a center position slightly west of Paul. Therefore, a simple addition of the spunup vortex for Paul to the environmental flow may cause undesirable dynamical adjustment problems.

b. Experimental design

In addition to the control simulation (CTL) conducted with the above-mentioned initialization method, three other experiments are performed to diagnose the motion of TS Rachel and different rainfall mechanisms associated with the storm (Table 1). In experiment NP, the circulation of TS Paul is removed from the ECMWF analysis using the Kurihara filtering, but no synthetic vortex is replaced. Therefore, only the monsoon gyre interacts with Rachel. Since the monsoon gyre is such a dominating synoptic system during the development of the two TSs, its effect is investigated by further removing the trough in the monsoon gyre in experiment NTR. The experiment has been conducted via a procedure described in Wu et al. (2009) for monsoon strength modification and will not be repeated in details here. The basic idea is first to reduce the low-level relative vorticity associated with the trough, and then to obtain the new streamfunction and wind field. By solving the nonlinear balance equation and hydrostatic equation the new geopotential height and temperature are also available for model initialization. The third sensitivity experiment, NTE, is the same as CTL except that Taiwan terrain height is assigned zero in order to look into topographic effects on the movement of Rachel and its associated rainfall. In addition, the difference between the simulated

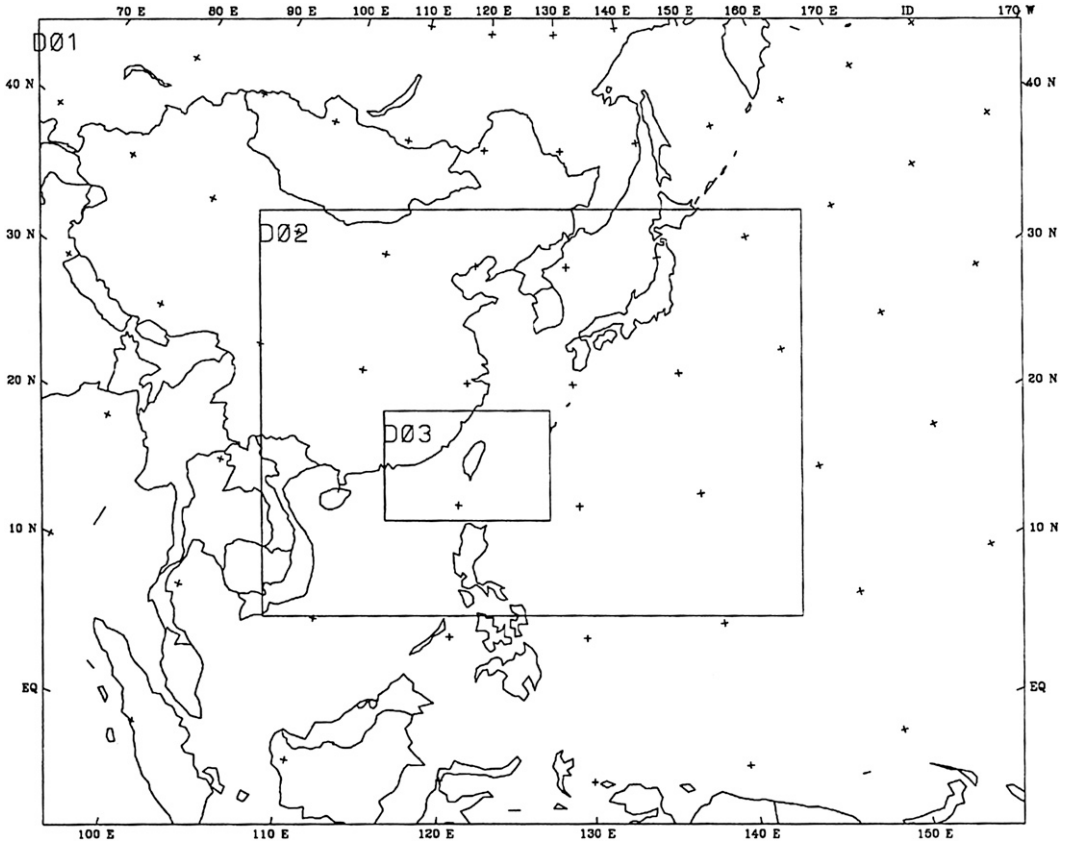

FIG. 3. The coarse and nested domains in the MM5 model with horizontal resolution of 54, 18, and 6 km, respectively.

results from CTL and NP (denoted as NMT) is examined in the next section to eliminate the effect from the monsoon trough.

4. Potential vorticity analysis

a. ECMWF data analyses

Piecewise potential vorticity (PV) inversion as applied in Wu et al. (2003, 2004) is used to diagnose the respective impact of TS Paul and the monsoon trough to the movement of TS Rachel. Application of the Ertel PV concept to weather systems diagnosis benefits largely from its invertibility principle, which states that the balanced mass and wind fields associated with a given PV distribution can be recovered by prescribed balanced condition and boundary conditions (Davis and Emanuel 1991). If the flow field is appropriately divided into the mean and perturbation components, then piecewise PV inversion can be used to obtain the balance fields

TABLE 1. Numerical experiments performed in this study with the same set of nested domains and horizontal resolution. Refer to the text for details of the vortex initialization methodologies.

Expt name	Description	Initialization method	Horizontal resolution		
			54 km	18 km	6 km
CTL	Control experiment	Rachel: SV+KF Paul: SV	E54CTL	E18CTL	E6CTL
NP	Circulation of TS Paul filtered from analysis	Rachel: SV+KF	E54NP	E18NP	E6NP
NMT	CTL minus NP (no monsoon trough)				
NTR	Both TS Paul and monsoon trough filtered	Rachel: SV+KF	E54NTR	E18NTR	E6NTR
NTE	No Taiwan terrain	Rachel: SV+KF Paul: SV	E54NTE	E18NTE	E6NTE

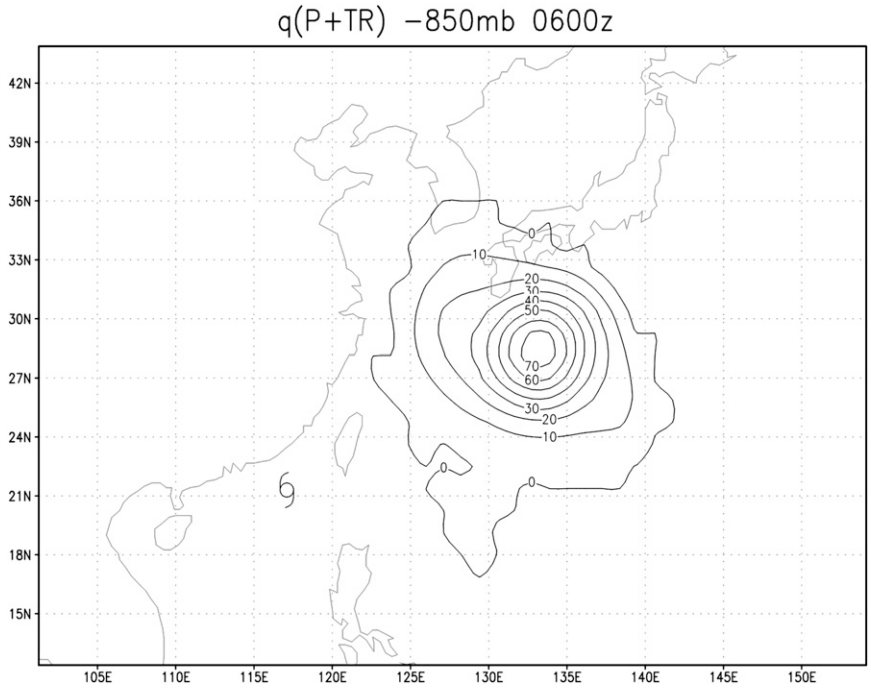

FIG. 4. 850-hPa PV perturbation at 0000 UTC 6 Aug associated with TS Paul and the monsoon trough derived from ECMWF analysis (unit: 0.01 PVU; 1 PVU $\equiv 10^{-6}$ m^2 s^{-1} K kg^{-1}).

associated with each individual PV perturbation (Davis 1992).

The climatological PV value is first used as the mean field for piecewise PV inversion analysis of the synoptic system (Wu and Emanuel 1995a,b), which cannot fully address the transient nature of TCs. Shapiro (1996) devised the new decomposition between the axisymmetric vortex as the mean field and the remaining as perturbation. Wu et al. (2003) further extended this decomposition for binary vortex interaction by taking the axisymmetric part of one vortex as the mean field, and further divide the perturbation field into one that is associated with the second vortex and the other with the environmental flow, respectively. In a similar manner for the two cyclones in this study, the axisymmetric PV component at 850 hPa of Rachel is taken as the mean field while the remaining PV is denoted as q' (which contains the asymmetric part of Rachel). The contributions from Paul and the monsoon trough only, termed $q'_{\mathrm{P+TR}}$, is then isolated by ignoring Rachel's asymmetric part (Fig. 4). The difference between q' and $q'_{\mathrm{P+TR}}$ [denoted $q'_{n(\mathrm{P+TR})}$] is therefore the PV perturbation component without influence of Paul and the monsoon trough.

As a consequence, the deep-layer-mean (925–400 hPa) steering vector for Rachel during 0000 UTC 6–8 August is defined as

$$\mathbf{V}_{\mathrm{SDLM}} = \frac{\int_{925\mathrm{hPa}}^{400\mathrm{hPa}} \mathbf{V}_S(p)\, dp}{\int_{925\mathrm{hPa}}^{400\mathrm{hPa}} dp},$$

where

$$\mathbf{V}_S(p) = \frac{\int_0^{3^\circ}\int_0^{2\pi} \mathbf{V} r\, d\theta\, dr}{\int_0^{3^\circ}\int_0^{2\pi} r\, d\theta\, dr}$$

is the azimuthally averaged wind vector within a radius of 3° latitude–longitude from the center of Rachel. The purpose of calculating this steering vector is to compare it with the PV-inverted wind vectors associated with different perturbation components so that relative contributions from these perturbation components can be measured. Quantitatively, an along-track projection (AT) of the deep-layer-mean steering vector associated with $q'_{\mathrm{P+TR}}$ onto the best-track motion vector is calculated as follows:

$$\mathrm{AT}(q'_{\mathrm{P+TR}}) = \frac{\mathbf{V}_{\mathrm{SDLM}}(q'_{\mathrm{P+TR}}) \cdot \mathbf{V}_{\mathrm{BT}}}{|\mathbf{V}_{\mathrm{BT}}|^2},$$

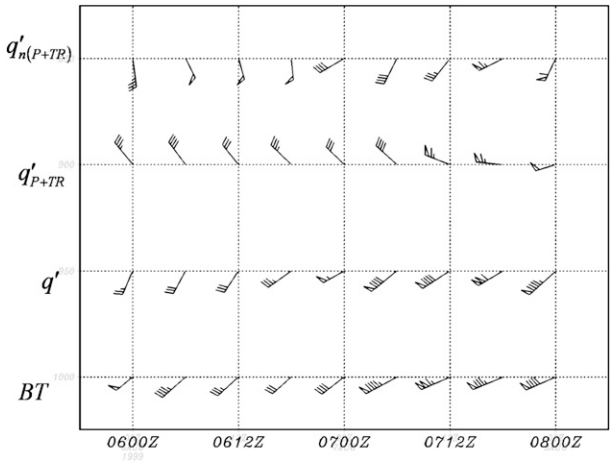

FIG. 5. 6-hourly deep-layer-mean (925–400 hPa) steering vectors within 3° latitude–longitude from the storm center derived from the motion vector of TS Rachel (BT), total PV perturbation (q'), PV perturbation associated with TS Paul and the monsoon trough ($q'_{\mathrm{P+TR}}$), and PV perturbation excluding TS Paul and the monsoon trough [$q'_{n(\mathrm{P+TR})}$] based on ECMWF analyses. Full barb represents 1 m s^{-1}.

which measures if the balanced wind field from perturbation of Paul and the monsoon trough facilitates Rachel's motion (positive AT) or opposes to it (negative AT). This projected speed ratio for the total PV perturbation and that excluding Paul and the monsoon trough, i.e., AT(q') and AT[$q'_{n(\mathrm{P+TR})}$], can be calculated in similar ways. Based on the definition of the linear superposition of PV, the sum of AT($q'_{\mathrm{P+TR}}$) and AT[$q'_{n(\mathrm{P+TR})}$] equals AT(q').

Detailed examination of the 6-hourly $\mathbf{V}_{\mathrm{SDLM}}(q'_{\mathrm{P+TR}})$ and $\mathbf{V}_{\mathrm{SDLM}}[q'_{n(\mathrm{P+TR})}]$ in Fig. 5 shows that Paul and the monsoon trough brought northwesterlies to the vicinity of Rachel from 0600 UTC 6 August to 1200 UTC 7 August, immediately after the storm made its landfall in Taiwan, indicating that these two systems were largely responsible for the deceleration of Rachel in this period. After 0600 UTC 7 August, steering vector associated with $q'_{\mathrm{P+TR}}$ starts to intensify in the westerly component and becomes more aligned with that associated with q' or the best-track direction, and thus Rachel moved much faster after passing through Taiwan. On the other hand, the steering vector associated with $q'_{n(\mathrm{P+TR})}$ has a considerably strong southwesterly or southerly component that is consistent with the fact that other than perturbations from Paul and the monsoon trough, the remaining PV field is derived from the monsoonal southwesterlies.

The AT values defined above confirm this subjective comparison of steering vector directions. AT($q'_{\mathrm{P+TR}}$) is negative until 1200 UTC 6 August, and gradually turns positive until 0600 UTC 7 August (Table 2). This

TABLE 2. Dimensionless values of the along-track projection of the deep-layer-mean (925–400 hPa) steering vector associated with total PV perturbation (q') onto the motion vector of TS Rachel. The total PV perturbation (q') is associated with $q'_{\mathrm{P+TR}}$ (TS Paul and the monsoon trough) and $q'_{n(\mathrm{P+TR})}$ (excluding TS Paul and the monsoon trough) in the ECMWF analyses.

Time	AT(q')	AT($q'_{\mathrm{P+TR}}$)	AT[$q'_{n(\mathrm{P+TR})}$]
0000 UTC 6 Aug	0.49	−0.52	1.11
0600 UTC 6 Aug	0.68	−0.50	0.88
1200 UTC 6 Aug	0.86	−0.29	1.03
1800 UTC 6 Aug	1.19	0.19	0.65
0000 UTC 7 Aug	1.47	0.16	0.67
0600 UTC 7 Aug	0.92	0.09	0.41
1200 UTC 7 Aug	0.79	0.45	0.37
1800 UTC 7 Aug	1.24	0.48	0.61
0000 UTC 8 Aug	1.00	0.47	0.58

projected speed ratio increases substantially to 0.45, 0.48, and 0.47 in the next 18 h when Paul moved more westward to the north of Rachel. The AT[$q'_{n(\mathrm{P+TR})}$] values show that the southwesterly monsoonal steering dominates the motion of Rachel to a certain extent until 0000 UTC 7 August, after which the effect of Paul and the monsoon trough adds in with comparable contributions from both perturbation components.

b. MM5 simulations

While the ECMWF analyses provide reliable observational data for the piecewise PV inversion calculation, it is not considered feasible to further separate the respective contributions from TS Paul and the monsoon trough to the motion of TS Rachel, and hence numerical simulations are carried out. In addition, since a shortwave trough passing through areas north or northeast of Taiwan is a relatively common phenomenon but not only observed in the monsoon gyre synoptic pattern as shown in this study, it is desirable to measure the quantitative influence of such a trough on the development of a TC that originates from the SCS.

The experiment for simulation NP without the vortex of Paul is designed for this purpose. Instead of assigning the axisymmetric component of Rachel as the mean PV field, the simulated PV in experiment NP that includes contribution from the monsoon trough is used. Since the total PV field is simulated in experiment CTL, NMT (i.e., the difference between CTL and NP) represents the PV perturbation associated with Paul but excludes the monsoon trough. For example, the initial 850-hPa PV field for experiment CTL at 0000 UTC 6 August shows a maximum value of about 0.85 PV unit (PVU) at the center of Paul (Fig. 6a). The maximum value in the initial PV field in experiment NP is only about 0.45 PVU and the area of maximum PV associated with the monsoon trough is northwest of TS Paul (Fig. 6b). When the

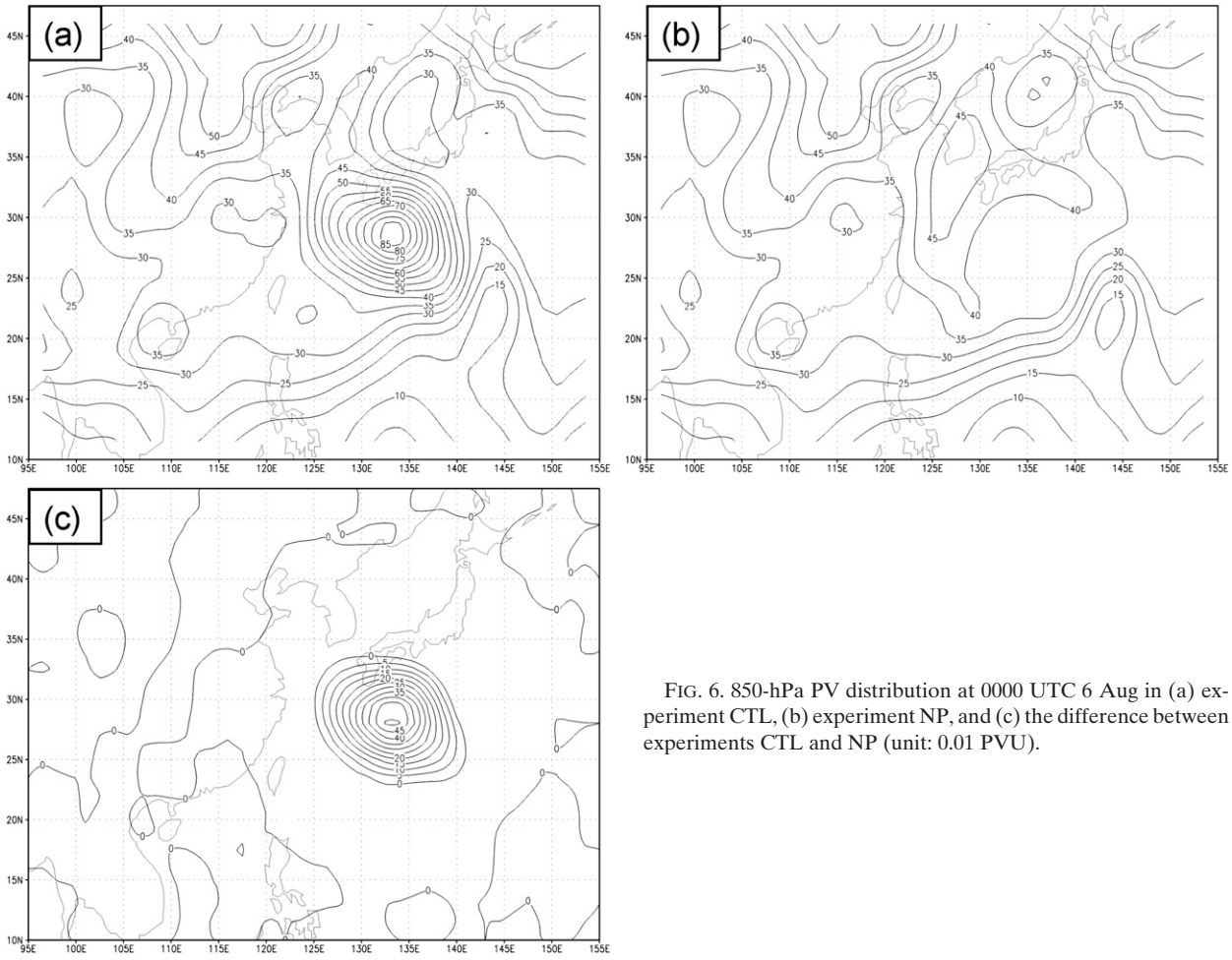

FIG. 6. 850-hPa PV distribution at 0000 UTC 6 Aug in (a) experiment CTL, (b) experiment NP, and (c) the difference between experiments CTL and NP (unit: 0.01 PVU).

differences between the initial PV fields and these two experiments are obtained, the near-axisymmetric PV perturbation of Paul is found to have a maximum value of about 0.45 PVU, similar to that in the monsoon trough (Fig. 6c).

Balanced wind fields associated with the PV perturbation of Paul and that associated with the total PV field in experiments CTL and NP are computed, respectively. Then the deep-layer-mean steering vectors for these inverted wind fields are also obtained as in the previous section (and hence the steering vectors resulted from the PV fields in experiments CTL and NP are similar to the simulated speed of Rachel in these two experiments). It is found that in the first 18-h simulation, the steering vectors in experiments CTL and NP are similar in both direction and magnitude because the contribution from Paul in this period is still minor (Fig. 7). Afterward, the magnitude of the steering vector associated with Paul increases, and without the influence from Paul, the motion of Rachel in experiment NP begins to deviate in direction and slow down compared with its counterpart in CTL. It is interesting to note that the steering vector associated with Paul has a southward component throughout the 48-h simulation time (i.e., Paul's influence always opposes to the northward movement of Rachel). On the other hand, the zonal component is very small initially and increases gradually toward the east in the later simulation period, thus facilitating the eastward motion of Rachel.

Furthermore, the PV perturbation associated with the monsoon trough has been identified and removed from the initial condition of experiment NTR. Piecewise inversion is also performed for the isolated PV perturbation of the monsoon trough to obtain its balanced wind field and the deep-layer-mean steering vector. The along-track projection of steering vectors onto the best-track motion vector of Rachel (i.e., the AT value defined previously) are also computed for Paul's PV perturbation and that of the monsoon trough (Fig. 8). It can be seen that in accordance with the qualitative examination in Fig. 7, the influence from Paul is minor before the landfall of Rachel at about 0600 UTC 7 August because AT(q'_P) is close to zero in the first 24-h simulation and increases

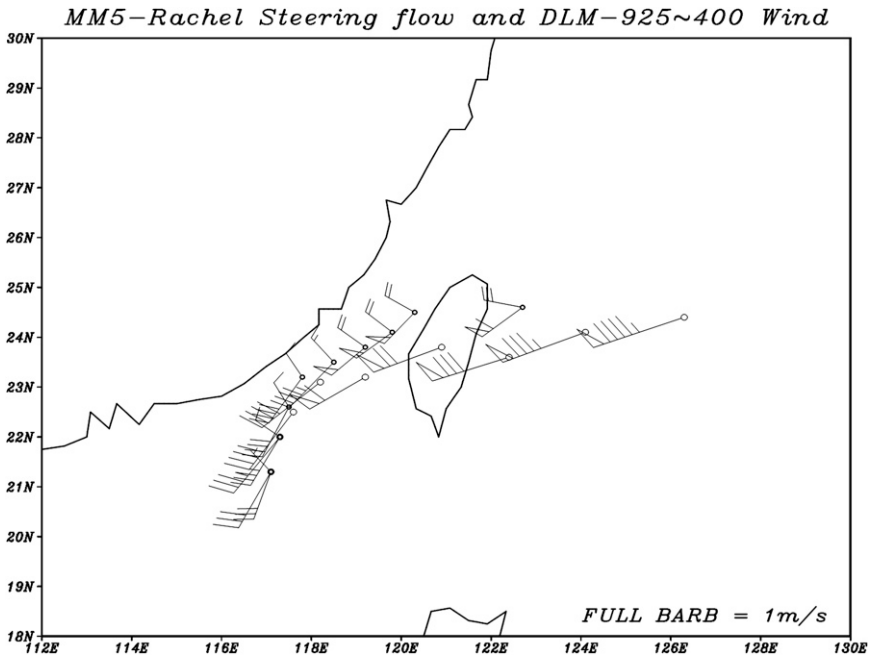

FIG. 7. 6-hourly deep-layer-mean (925–400 hPa) steering vectors within 3° latitude–longitude from the storm center derived from the total PV field in experiment CTL (long barb), the total PV field in experiment NP (medium barb), and the difference in PV between the experiments CTL and NP (short barb). The latter two are located at the simulated positions of TS Rachel in experiment NP that are different from those in experiment CTL (see also Fig. 9). Full barb represents 1 m s^{-1}.

only afterward. In contrast, the monsoon trough actually plays an important role in decelerating Rachel [negative AT(q'_{TR})] in the first 18 h as well as in accelerating it afterward [positive AT(q'_{TR})].

In summary, PV diagnosis of the ECMWF analyses and MM5 simulations depicts varying influences of Paul and the monsoon trough, both negative and positive, on the motion of Rachel before and after landfall. While influence from Paul always opposes the northward migration of Rachel throughout the analysis period, impediment to eastward motion initially comes from the monsoon trough and results in a slowdown/deceleration of Rachel. Then during landfall in and passage through Taiwan, comparable steering comes from both Paul and the monsoon trough.

c. *Simulated storm tracks*

The simulated tracks in all sensitivity experiments performed are examined because they are crucial to the variability in the simulated rainfall distribution that will be discussed in the next section. The simulated motion of TS Rachel agrees well with the best track in terms of its deceleration before landfall in Taiwan and the subsequent acceleration after moving back to the ocean, but with a general southward bias in the final 24-h simulation (Fig. 9). The omission of Taiwan's terrain in experiment NTE does not change much the simulated track of Rachel for the reason discussed in the previous section. The monsoon trough influences the storm's motion substantially and the CMR may not be the

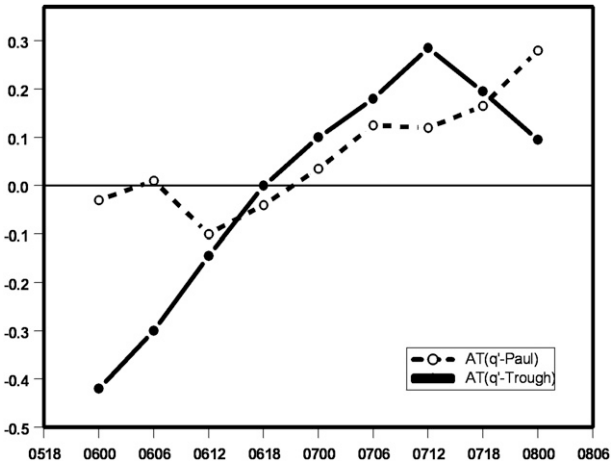

FIG. 8. Time series of the dimensionless along-track projection of certain deep-layer-mean steering vectors onto the motion vector of TS Rachel. The vectors projected are associated with the PV perturbation which is in turn either associated with TS Paul or monsoon trough and are derived from MM5 simulations. Time is denoted as "ddhh" where "dd" is the date in August and "hh" is the UTC time.

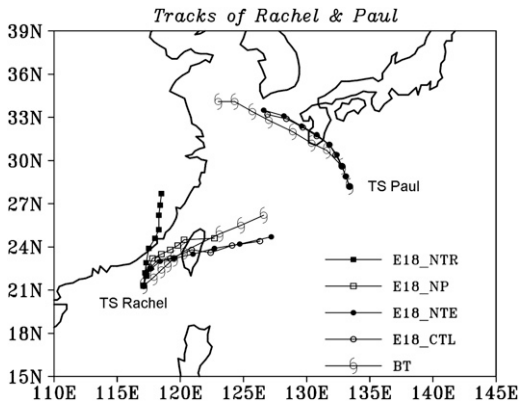

FIG. 9. JTWC best tracks (BT) and the MM5-simulated tracks of TSs Rachel and Paul derived from the 18-km horizontal resolution domain of the experiments CTL, NP, NTR, and NTE.

dominating factor in decelerating the storm. As pointed out in Lin et al. (2002), the CMR often forces wind flow from weak storms to detour round instead of going over mountains and causes discontinuity in the track as seen in the simulation of experiment CTL. The influence of the monsoon trough on Rachel's motion can be confirmed again when the simulated track in experiment NTR is examined. It is shown in experiment NTR that Rachel migrates nearly northward according to the monsoonal southerlies and makes landfall at southeast China instead of Taiwan. For TS Paul, simulated tracks in experiments CTL and NTE are once again similar, and both show similar southern bias as compared with the best track.

Since it is well recognized that uncertainties exist in the intensity of best-track data, detailed verification of the simulated intensity of Rachel is not performed in the study. It suffices to document that in the first 24-h simulation, the simulated mean sea level pressures of Rachel in experiment CTL and other sensitivity experiments (except NTR) are slightly lower than that analyzed by the Japan Meteorological Agency by 6–8 hPa. In the subsequent 24 h, the simulated Rachel in these experiments weakens but deviation from the analyzed mean sea level pressure is within 5 hPa. Nevertheless, since the simulated intensities in all sensitivity experiments (except NTR in which Rachel makes landfall too early and weakens rapidly) are similar, variability in simulated rainfall is not attributed too much to variability in storm intensity but to different physical processes that generate or prohibit rainfall.

5. Rainfall sensitivity

a. Influence of TS Paul on rainfall

In addition to the well-forecasted track, experiment CTL also simulates rainfall evolution similar to that observed. During 1200 UTC 6 August–0000 UTC 7 August when Rachel is still in the SCS, rainfall starts to appear in southwestern Taiwan. However, a comparison with the observed accumulated rain in this period (cf. Figs. 2a and 10a) shows that more rainfall is expected in the southern CMR area. An examination of the simulated low-level flow depicts two branches: one within the circulation associated with Rachel, which has a southerly flow moving northward almost in parallel to the CMR and is thus not lifted by topography; the other a branch of monsoonal southwesterly hitting the southern CMR (Fig. 10d). The underprediction of rainfall in this area may be due to the terrain height not adequately resolved in the MM5 model. Studies such as Yeh and Chen (2002) also discussed the convergence of the two branches of flow in northeastern Taiwan that leads to heavy rainfall. However, the moderate intensity of Rachel does not create strong low-level convergence in the simulation. When the simulated Rachel makes landfall and moves over the CMR during 0000–1200 UTC 7 August, the embedded convection generates rainfall in central Taiwan. Since moisture is kept at the western side of CMR, orographic lifting also generates convection and enhances rainfall (Figs. 10b,e). In the next 12 h, when Rachel moves back to the ocean and when the eastern side of the CMR becomes windward side again, little rain is simulated, the phenomenon of which is consistent with observations (cf. Figs. 2c and 10c). Experiment CTL successfully simulates the dry environment on the eastern side of the CMR (Fig. 10f), because the huge volume of moisture blocked on the western side turns into precipitation (Figs. 14d–f). In addition, when the relatively dry airflow moves over the CMR, subsidence and adiabatic warming keep the environment even drier.

In contrast to the results of CTL, deceleration of the simulated Rachel vortex in experiment NP leads to changes in rainfall distribution especially at later stages of the simulation. Because the simulated Rachel of NP stays longer in the Taiwan Strait, its cyclonic flow structure is well maintained until about 1200 UTC 7 August. However, its low-level flow at the northern side is very dry (relative humidity below 60%) due to the influence of the Taiwan terrain and probably due to dry air from South China as well (Fig. 11a). Since the simulated position in NP is north of that in CTL, moist southwesterly monsoonal flow has the channel to impinge into the CMR and generate rainfall by orographic lifting. Despite these changes in simulated track of Rachel, the accumulated rainfall during 0000–1200 UTC 7 August in experiment NP still considerably resembles that observed with maxima near central and northern CMR (cf. Figs. 2b and 11c). The impact of the removal of Paul in this experiment increases in the following 12 h.

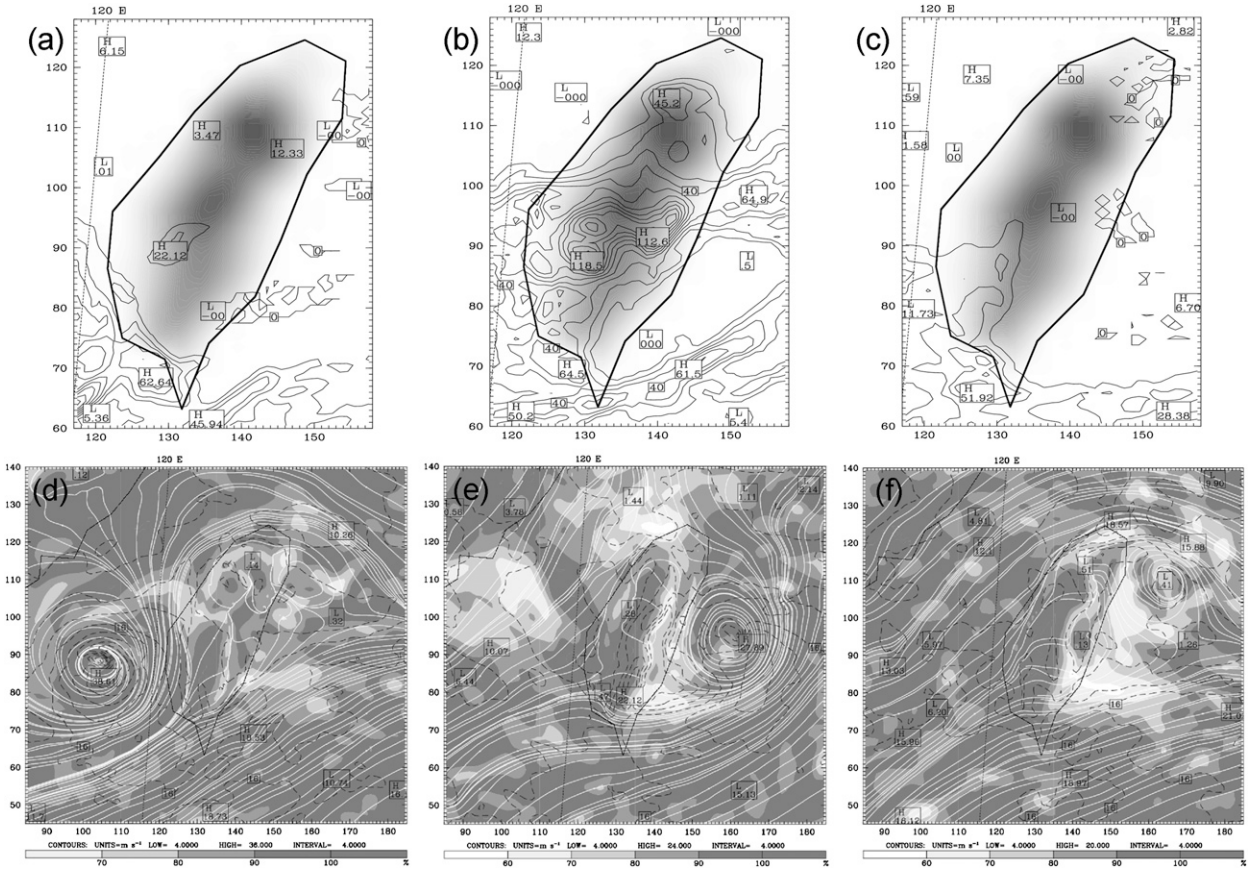

FIG. 10. Topography (shaded) and simulated accumulated rainfall (contour, mm) during (a) 1200 UTC 6 Aug–0000 UTC 7 Aug, (b) 0000–1200 UTC 7 Aug, and (c) 1200 UTC 7 Aug–0000 UTC 8 Aug in experiment CTL. Simulated 925-hPa flow, wind speed (dashed), and relative humidity (shaded) at (d) 0000 UTC 7 Aug, (e) 1200 UTC 7 Aug, and (f) 0000 UTC 8 Aug in the same experiment.

Because the simulated Rachel merely crosses Taiwan near the end of the simulation period, more CMR dry air (again with relative humidity much lower than 60%) due to subsidence and adiabatic warming is accumulated at the eastern side, entrained into Rachel's circulation and weakening the storm substantially (Fig. 11b). Because of this sharp division of moisture between both sides of the CMR and northward bias of the simulated storm center, the maximum accumulated rainfall during 1200 UTC 7 August–0000 UTC 8 August is recorded in northwestern Taiwan and is overestimated when compared with observations (cf. Figs. 2c and 11d).

As has been discussed earlier, the simulated track of Rachel in experiment NTR deviates much from the CTL due to filtering of the monsoon trough. A similar situation applies to the simulated rainfall, which is not further discussed here.

b. Topographic influence on rainfall

Mechanisms of the topographic influence on TC rainfall have been investigated in a number of previous studies such as Lin et al. (2001, 2002) and Wu et al. (2002). The environmental conditions favorable for heavy orographic rainfall to occur have also been identified. While the simulation results from the sensitivity experiments in this study are all consistent with the mechanisms discussed in the previous studies, emphasis is put on the topographic influence on moisture transport in the case of TS Rachel by comparing experiments NTE (no terrain) and CTL.

As shown in Fig. 9, the simulated track of Rachel in experiment NTE is almost identical to that in experiment CTL except for some slight fast bias. Previous studies such as Bender et al. (1985, 1987), Wu (2001), and Yeh and Elsberry (1993a,b) investigated the influences from terrain on the TC track including separation of low-level and upper-level vortex centers, formation of secondary low, and discontinuity in track. The similarity of the simulated tracks of Rachel in NTE and CTL suggests that these effects may be minimal for Rachel because of the strong steering effect from both Paul and the monsoon trough as diagnosed in the

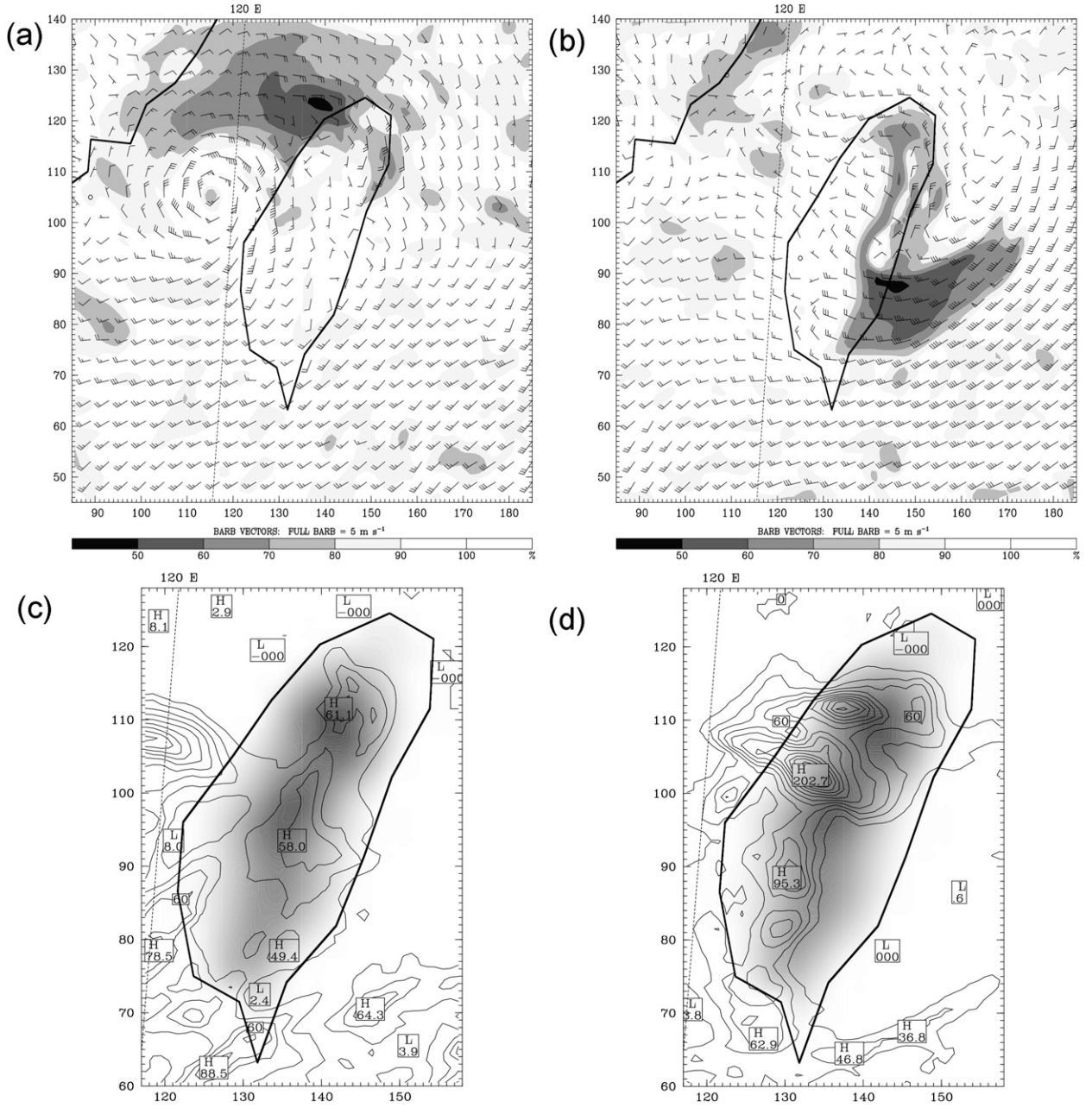

FIG. 11. Simulated 925-hPa relative humidity (shaded) and wind field (full barb 5 m s^{-1}) at (a) 1200 UTC 7 Aug and (b) 0000 UTC 8 Aug in experiment NP. Topography (shaded) and simulated accumulated rainfall (contour, mm) during (c) 0000–1200 UTC 7 Aug and (d) 1200 UTC 7 Aug–0000 UTC 8 Aug in the same experiment.

previous section. Again, because of the similar tracks in the two experiments (NTE and CTL), differences in other simulated physical processes such as rainfall should be attributed to lack of terrain in NTE (but still maintaining the land–sea contrast).

As no terrain blocks Rachel's low-level flow and associated moisture in experiment NTE, simulated rainfall is only distributed along its track during landfall (Fig. 12a) and decreases rapidly after the storm leaves the island without enhancement effect from orographic lifting of the monsoonal flow (Fig. 12b). The simulated maximum rainfall of about 70 mm during 0000–1200 UTC 7 August is only about half of that in experiment CTL. Idealized numerical studies of landfalling TCs such as Chan and Liang (2003) indicated concentration of convection ahead and on the right-hand side of the storm

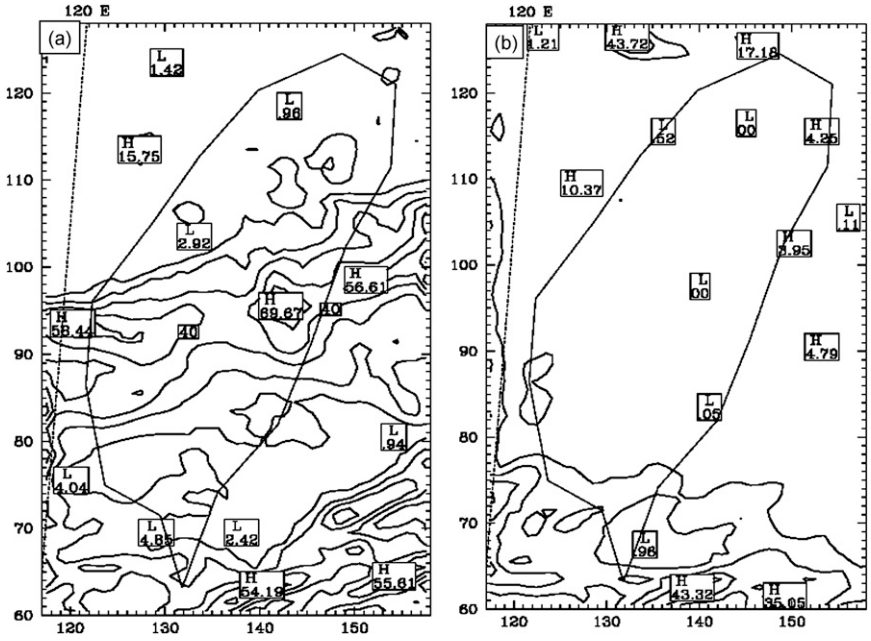

FIG. 12. Simulated accumulated rainfall (mm) during (a) 0000–1200 UTC 7 Aug and (b) 1200 UTC 7 Aug–0000 UTC 8 Aug in experiment NTE.

track. Not much asymmetry in precipitation of Rachel in experiment NTE is identified probably because Taiwan only covers part of the storm's circulation and the land–sea contrast is not substantial, and that a dry area developing within Rachel suppresses rainfall on the right-hand side of its track (Figs. 13a–c).

Detailed comparison of the development of low-level moisture in experiments NTE and CTL clearly depicts the topographic effect on the transport of moisture in Rachel. As early as 0000 UTC 7 August, relatively dry areas are found at the east side of Taiwan in CTL due to the blocking of moisture by the CMR and subsidence of air before the landfall of Rachel. Similar dry areas are not found in NTE because moisture can be transported eastward by Rachel's circulation and northeastward by the enhanced monsoonal southwesterlies (Figs. 13a,d). Examination of the vertical velocity at a zonal cross section through the center of the storm shows its asymmetric structure: strong convection concentrates ahead of the storm center with moist air transported upward to 300 hPa in both experiments NTE and CTL suggests that instead of topographic effect, this is intrinsic asymmetry within the storm (Figs. 14a,d). Six hours later when Rachel starts to make landfall, its storm structure is maintained in NTE, but is greatly disorganized by topography in CTL (Figs. 13b,e). Moreover, dry air originating from South China is advected into the eastern and southeastern side of Rachel in both experiments, which is an additional factor affecting the storm development. However, the responses of Rachel in the two experiments are totally different. In CTL, the level of maximum vertical velocity is raised by topography to about 700 hPa, moist air continues to be advected to upper levels and air subsides at the eastern side of CMR (Fig. 14e). On the other hand, convection ahead of storm is largely shut down in NTE because of the reduced moisture flux over land and therefore upper-level dry air gradually extends eastward (Fig. 14b). At 1200 UTC 7 August when Rachel again moves over the ocean, the east–west contrast in humidity over Taiwan develops (Figs. 13f and 14f). In other words, the topographic effect of moisture redistribution surpasses that of dry air intrusion from the east, and results in a rainfall pattern that is highly correlated to the terrain. Since no moisture redistribution mechanism exists in experiment NTE, dry air in the Taiwan Strait continues to be advected eastward and distributed in central Taiwan (Figs. 13c and 14c).

6. Summary

A numerical study is performed on the heavy rainfall event associated with the passage of TS Rachel over southern Taiwan with a specific purpose of examining the conceptual model proposed in Lin et al. (2001), in which the presence of TS Paul plays a dominating role in impeding the movement of Rachel, and thus is also one of the key factors that enhance rainfall amount in southern

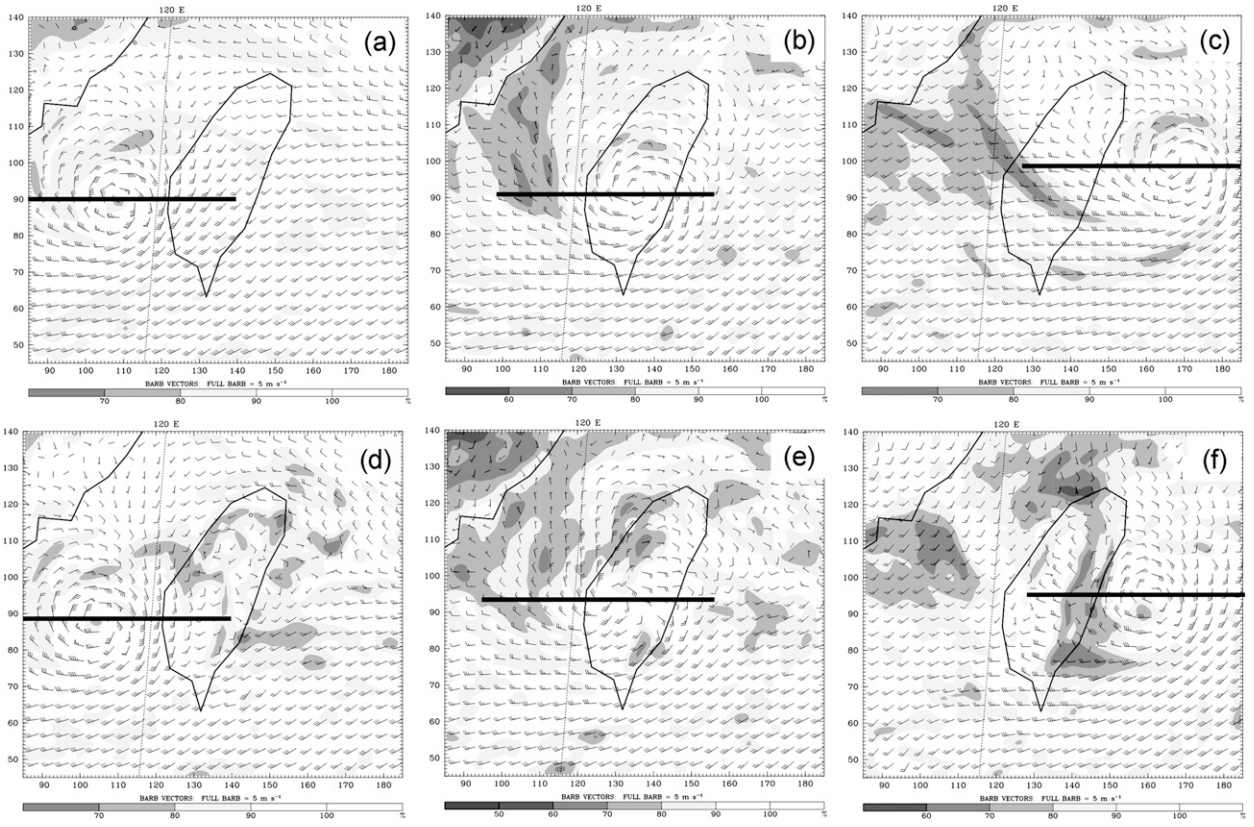

FIG. 13. Simulated 925-hPa relative humidity (shaded) and wind field (full barb 5 m s^{-1}) at (a) 0000 UTC 7 Aug, (b) 0600 UTC 7 Aug, and (c) 1200 UTC 7 Aug in experiment NTE. (d)–(f) As in (a)–(c), but are based on data from experiment CTL.

Taiwan. First, potential vorticity inversion is applied to ECMWF analyses for diagnosing the motion of Rachel. It is found that the combined effect of Paul and the trough embedded in the monsoon gyre synoptic pattern slows down the northward motion of Rachel before landfall in accordance with the deceleration in translation speed as observed in best-track data. Afterward, Rachel is steered eastward and then northeastward by these two systems across Taiwan.

To distinguish the contributions from Paul and the monsoon trough to the steering of Rachel, control and sensitivity experiments utilizing the MM5 model are performed by removing the circulation of Paul, and/or the monsoon trough system in which Paul is imbedded. Potential vorticity diagnosis of these simulations shows that while the movement of Rachel is indeed affected by the presence of Paul, its degree of influence is relatively small immediately before Rachel makes landfall. Nevertheless, it is the presence of the entire monsoon trough that impedes the movement of Rachel initially, steers the storm toward southwestern Taiwan especially near landfall, and also assists in the storm's passage through Taiwan.

The simulation results in this study support the conceptual model on the heavy rainfall mechanism as proposed in Lin et al. (2001), and are consistent with other environmental conditions of heavy orographic rain discussed in other studies. Moreover, our analyses based on the comparison between simulations with and without Taiwan terrain show that when the moisture-laden air from the SCS associated with Rachel and the southwesterly monsoon impinges upon the CMR and accumulates moisture there, relatively dry air from South China moved into Rachel's circulation. The role played by Taiwan's terrain is to force convection on the windward side and lead to subsidence on the lee side, thus creating an east–west partition of moisture and rainfall. This orographic effect eventually surpasses the dry region that originally develops into Rachel, and results in the observed rainfall distribution. Therefore, it is concluded that the existence of terrain would modify the low-level circulation of passing TCs, generating secondary circulation and enhancing windward side convection, while the interplay with other potential synoptic and mesoscale systems would modulate the detailed heavy rainfall distribution.

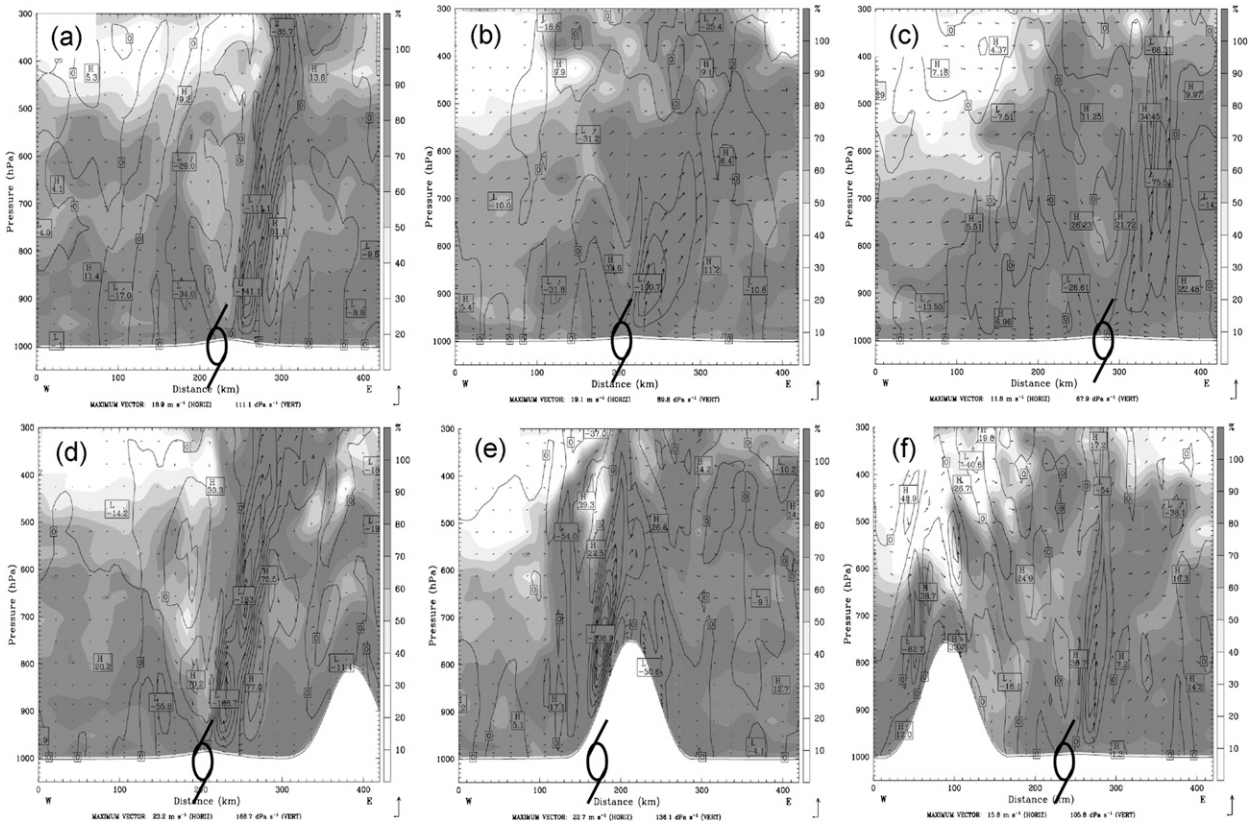

FIG. 14. Simulated relative humidity (shaded), vertical velocity (contour, Pa s^{-1}), and zonal and vertical wind components (vector) at (a) 0000 UTC 7 Aug, (b) 0600 UTC 7 Aug, and (c) 1200 UTC 7 Aug in experiment NTE. (d)–(f) As in (a)–(c), but are based on data from experiment CTL.

Acknowledgments. The work is supported by National Science Council Grant NSC95-2119-M-002-039-MY2 and National Taiwan University Grant NTU-97R0302.

REFERENCES

Bender, M. A., R. E. Tuleya, and Y. Kurihara, 1985: A numerical study of the effect of a mountain range on a landfalling tropical cyclone. *Mon. Wea. Rev.,* **113,** 567–582.

——, ——, and ——, 1987: A numerical study of the effect of island terrain on tropical cyclones. *Mon. Wea. Rev.,* **115,** 130–155.

Blackadar, A. K., 1979: High resolution models of the planetary boundary layer. *Advances in Environmental Science and Engineering,* J. Pfafflin and E. Ziegler, Eds., Vol. 1, Gordon and Breach, 50–85.

Chan, J. C. L., and X. Liang, 2003: Convective asymmetries associated with tropical cyclone landfall. Part I: *f*-plane simulations. *J. Atmos. Sci.,* **60,** 1560–1576.

Cheung, K. K. W., L.-R. Huang, and C.-S. Lee, 2008: Characteristics of rainfall during tropical cyclone periods in Taiwan. *Nat. Hazards Earth Syst. Sci.,* **8,** 1463–1474.

Chiao, S., and Y. L. Lin, 2003: Numerical modeling of an orographically enhanced precipitation event associated with Tropical Storm Rachel over Taiwan. *Wea. Forecasting,* **18,** 325–344.

Chien, F.-C., Y.-C. Liu, and C.-S. Lee, 2008: Heavy rainfall and southwesterly flow after the leaving of Typhoon Mindulle (2004) from Taiwan. *J. Meteor. Soc. Japan,* **86,** 17–41.

Davis, C. A., 1992: Piecewise potential vorticity inversion. *J. Atmos. Sci.,* **49,** 1397–1411.

——, and K. A. Emanuel, 1991: Potential vorticity diagnostics of cyclogenesis. *Mon. Wea. Rev.,* **119,** 1929–1953.

Doswell, C. A., III, H. Brooks, and R. Maddox, 1996: Flash flood forecasting: An ingredient-based methodology. *Wea. Forecasting,* **11,** 560–581.

Dudhia, J., 1993: A nonhydrostatic version of the Penn State/NCAR mesoscale model: Validation tests and simulation of an Atlantic cyclone and cold front. *Mon. Wea. Rev.,* **121,** 1493–1513.

Grell, G. A., 1993: Prognostic evaluation of assumptions used by cumulus parameterization. *Mon. Wea. Rev.,* **121,** 764–787.

Kurihara, Y., M. A. Bender, and R. J. Ross, 1993: An initialization scheme of hurricane models by vortex specification. *Mon. Wea. Rev.,* **121,** 2030–2045.

——, ——, R. E. Tuleya, and R. J. Ross, 1995: Improvements in the GFDL hurricane prediction system. *Mon. Wea. Rev.,* **123,** 2791–2801.

Lee, C.-S., Y.-C. Liu, and F.-C. Chien, 2008: The secondary low and heavy rainfall associated with Typhoon Mindulle (2004). *Mon. Wea. Rev.,* **136,** 1260–1283.

Lin, Y.-L., S. Chiao, T.-A. Wang, M. L. Kaplan, and R. P. Weglarz, 2001: Some common ingredients for heavy orographic rainfall. *Wea. Forecasting,* **16,** 633–660.

——, D. B. Ensley, S. Chiao, and C. Y. Huang, 2002: Orographic influences on rainfall and track deflection associated with the passage of a tropical cyclone. *Mon. Wea. Rev.,* **130,** 2929–2950.

McPherson, T., and W. Stapler, Eds., 1999: Annual tropical cyclone report. U.S. Naval Pacific Meteorology and Oceanography Center/Joint Typhoon Warning Center, Pearl Harbor, HI, 213 pp.

Reisner, J., R. M. Rasmussen, and R. T. Bruintjes, 1998: Explicit forecasting of supercooled liquid water in winter storms using the MM5 mesoscale model. *Quart. J. Roy. Meteor. Soc.,* **124,** 1071–1107.

Shapiro, L. J., 1996: The motion of Hurricane Gloria: A potential vorticity diagnosis. *Mon. Wea. Rev.,* **124,** 1363–1379.

Wu, C.-C., 2001: Numerical simulation of Typhoon Gladys (1994) and its interaction with Taiwan terrain using the GFDL hurricane model. *Mon. Wea. Rev.,* **129,** 1533–1549.

——, and K. A. Emanuel, 1995a: Potential vorticity diagnostics of hurricane movement. Part I: A case study of Hurricane Bob (1991). *Mon. Wea. Rev.,* **123,** 69–92.

——, and ——, 1995b: Potential vorticity diagnostics of hurricane movement. Part II: Tropical Storm Ana (1991) and Hurricane Andrew (1992). *Mon. Wea. Rev.,* **123,** 93–109.

——, and Y.-H. Kuo, 1999: Typhoons affecting Taiwan: Current understanding and future challenges. *Bull. Amer. Meteor. Soc.,* **80,** 67–80.

——, T.-H. Yen, Y.-H. Kuo, and W. Wang, 2002: Rainfall simulation associated with Typhoon Herb (1996) near Taiwan. Part I: The topographic effect. *Wea. Forecasting,* **17,** 1001–1015.

——, T.-S. Huang, W.-P. Huang, and K.-H. Chou, 2003: A new look at the binary interaction: Potential vorticity diagnosis of the unusual southward movement of Tropical Storm Bopha (2000) and its interaction with Supertyphoon Saomai (2000). *Mon. Wea. Rev.,* **131,** 1289–1300.

——, ——, and K.-H. Chou, 2004: Potential vorticity diagnosis of the key factors affecting the motion of Typhoon Sinlaku (2002). *Mon. Wea. Rev.,* **132,** 2084–2093.

——, K. K. W. Cheung, and Y.-Y. Lo, 2009: A numerical study of the heavy rainfall event due to the interaction of Typhoon Babs (1998) and the northeasterly monsoon. *Mon. Wea. Rev.,* **137,** 2049–2064.

Yeh, H.-C., and Y.-L. Chen, 2002: The role of offshore convergence on coastal rainfall during TAMEX IOP 3. *Mon. Wea. Rev.,* **130,** 2709–2730.

Yeh, T.-C., and R. L. Elsberry, 1993a: Interaction of typhoons with the Taiwan orography. Part I: Upstream track deflections. *Mon. Wea. Rev.,* **121,** 3193–3212.

——, and ——, 1993b: Interaction of typhoons with the Taiwan orography. Part II: Continuous and discontinuous tracks across the island. *Mon. Wea. Rev.,* **121,** 3213–3233.